CHALMERS

Modeling of Concentration Profiles in Yeast Capsules for Efficient Bioethanol Production

Numerical study of mass transfer effects in encapsulated yeast pellets using FEM simulations in Comsol Multiphysics 3.5a

Master of Science Thesis

RIANI AYU LESTARI

Department of Chemical and Biological Engineering
Industrial Biotechnology Group
CHALMERS UNIVERSITY OF TECHNOLOGY
Göteborg, Sweden, 2010

Modeling of Concentration Profiles in Yeast Capsules for Efficient Bioethanol Production

Numerical study of mass transfer effects in encapsulated yeast pellets using FEM simulations in Comsol Multiphysics 3.5a

RIANI AYU LESTARI,

Supervisor: Associate Prof. Carl Johan Franzén
Prof. Bengt Andersson
Examiner: Associate Prof. Carl Johan Franzén

Department of Chemical and Biological Engineering
Industrial Biotechnology
Chalmers University of Technology
SE-412 96 Göteborg
Sweden

Telephone + 46 (0)31-772 1000

ACKNOWLEDGEMENT

I am proud during I do master thesis in Industrial Biotechnology. I am, from Chemical Engineering try to look other things for adding knowledge and experiences by doing the master thesis in this division. As an exchange student in Linnaeus Palme Program, I get the chance to study more and be more confident for facing my future of study. A lot of thank which would be presented to many people for accompanying and supporting in multiple ways.

I would like to express my deep gratitude to Carl Johan Franzen (Calle) and Bengt Andersson as my supervisor for teaching, guidance, encouraging and his patience during my work. I hope we can meet in other chance and time. I thank to Claes Niklasson as a leader for Linnaeus-Palme program, good impression when we met in interview in Gadjah Mada University. I thank to Bengt Andersson for teaching and suggestion about computational fluid dynamics and programming.

I would also like to thank to staff at Industrial Biotechnology, Lisbeth Olson, Eva Albers and staff at Chemical Reaction Egineering, Marianne Sognell and Derek Creaser.

I am greateful to all people in Chalmers tekniska högskola for pleasant atmosphere. I would like to study hard and I wish I would be back here for studying. I also appreciate my friends in Laskar Göteborg group as a second family during I live in Sweden (*vi är bäst*!).

Finally, I wish to thank to my parent, my family in Indonesia for praying, for endless love even though so far distance between us.

Riani Ayu Lestari

2010-07-1

Modeling of Concentration Profiles in Yeast Capsules for Efficiency Bioethanol Production

Master Thesis

RIANI AYU LESTARI

Department of Chemical and Biological engineering

Division of Industrial Biotechnology

Chalmers University of Technology

ABSTRACT

Encapsulated yeast can be used for increasing bioethanol production during fermentation of inhibitory lignocellulose hydrolysates. It is useful for decreasing the effect of inhibitors when the substrate through the capsule. It can be considered as a spherical pored catalyst, which contains yeast within the capsule. The capsule has 3 main parts, i.e. capsule membrane, cell pellet and liquid core. Glucose consumption by encapsulated yeast was modeled as a diffusion and reaction process. The diffusion included effects of different diffusivities of the capsule membrane (Dm) and cell pellet (Dc). The reaction was assumed by following Monod kinetics. Comsol Multiphysics was used to simulate mass transfer effect in encapsulated cells using the finite element method. Simulation was set in 2D and geometry was set in axis symmetry. Steady state concentration profiles were obtained after 24 hours depending on the diffusivity in membrane and cell pellet. Steady state glucose limitation was only apparent if Dc or Dm was ≤ 1% of the diffusivity in water. However, temporary glucose limitation was observed after 1 and 2 hours cultivation in many cases. The internal diffusion is more affect to rate concentration limiting because of cell diffusivity.

Keywords: Simulation, Modeling, Diffusion-Reaction process, Encapsulated yeast, Comsol Multiphysics.

TABLE OF CONTENTS

1. INTRODUCTION

1.1 Background

Ethanol, both renewable and environmentally friendly, is believed to be one of the best alternative biofuels. This has led to a dramatic increase in its production capacity. Among many microorganism that have been exploited for ethanol production, *Saccharomyces cerevisiae* still remains as the prime species [1].

Ethanol can be produced from lignocellulosic raw materials. Main processes of ethanol production involve hydrolysis and fermentation [21]. Lignocellulosic materials are an abundant and renewable source of sugar substrate that could be fermented to ethanol for use as a fuel extender and chemical feedstock. The discovery of yeast species is able to ferment glucose, the hemicellulosic-derived sugar. Depending on a two- or single-stage hydrolysis process, glucose, derived from lignocellulose can be converted into ethanol by separated fermentations or by a coculture process by using, microorganisms. *Saccharomyces cerevisiae* has better ethanol yields and productivities from glucose [24].

During pretreatment and hydrolysis of lignocellulosic biomass, a great amount of compounds that can seriously inhibit the subsequent fermentation are formed in addition to fermentable sugars. Inhibitory substances are generated as a result of the hydrolysis of the extractive components, organic and sugar acids esterified to hemicellulose (acetic, formic, glucuronic, galacturonic), and solubilized phenolic derivatives. In the same way, inhibitors are produced from the degradation products of soluble sugars (furfural, HMF) and lignin (cinnamaldehyde, p-hydroxybenzaldehyde, syringaldehyde), and as a consequence of corrosion (metal ions) [8, 25]. For this reason and depending on the type of employed pretreatment and hydrolysis, detoxification of the streams that will undergo fermentation is required. Detoxification methods can be physical, chemical or biological. In addition, the fermenting microorganisms have different tolerances to the inhibitors.
While the free cells of *Saccharomyces cerevisiae* were not able to ferment the hydrolyzates within at least 24 hours, the encapsulated yeast successfully converted glucose and mannose in both of the hydrolyzates in less than 10 h with no significant lag phase [9].

Encapsulated yeast, or bioartificial organs, is used to enclose a wide range of yeast as bioactive materials which is carried out by using either natural or synthetic polymers such as

calcium alginate [17]. The latter permits the entry of nutrients and oxygen and the exit of therapeutic protein products. Furthermore, the semipermeable nature of the membrane prevents high molecular weight molecules, antibodies and other immunologic moieties from coming into contact with the encapsulated cells and destroying them as foreign invaders [26].

Cell encapsulation systems referred to as immunoprotective devices. For the formation of immunoprotective devices, cell encapsulation can be broadly classified into two categories: microencapsulation, defined as the enclosure of individual cells or small cell aggregates in a semipermeable membrane and macroencapsulation, which utilizes hollow semipermeable materials to deliver multiple cells or cell aggregates [27].

In addition, the encapsulated yeast has advantages, that are higher productivity, higher ethanol yield, lower yields of byproducts, high cell concentration, no lag phase, better tolerance against inhibitors, and leakage to the media.

The focus of the current work was to estimate glucose concentration profiles at several different relative diffusivities and different amounts of cells in the capsule by using modeling and simulating in Comsol multiphysics 3.5a.

1.1.1. Bioethanol as a fuel

Ethanol, also known as ethyl alcohol with the chemical formula C_2H_5OH, is a flammable, clear, colorless and slightly toxic chemical organic compound with acceptable odor. It can be produced either from petrochemical feedstock by the acid-catalyzed hydration of ethene, or from biomass feedstock through fermentation. On global scale, synthetic ethanol accounts for about 3-4% of total production while the rest is produced from fermentation of biomass – mainly sugar crops, e.g. cane and beet, and of grains [6].

1.1.2. Cell Encapsulation

Cell encapsulation has many techniques. Those are coaservation, interfacial polymerization, pregel dissolving and liquid droplet formation. Encapsulation concept is about coating a material, which is used in certain process and condition for preventing the leakage of the capsule.

The idea of using polymer membrane microcapsules was first begun by Chang since 1964 for immunoprotection of transplanted cells. He introduced the term of “artificial cells” for biologically active materials enclosed in a semipermeable membrane. The coating material, also called a capsule, membrane, carrier or shell, is generally composed of natural or synthetic polymers. The main reason for using polymers for encapsulation lies in their ability to exist at different phases as liquids, gels or solids, which enables them to meet a large range of mechanical and physical demands.

Encapsulated yeast is shown in figure below.

Figure 1.Encapsulated yeast

1.2 Purpose of Project

This thesis aims to study and evaluate concentration profiles and perform encapsulated cell simulation in Comsol. This could increase the understanding of:

1. Concentration gradient in capsule at different combinations of relative membrane and cell diffusivities
2. The dependence of the rate of glucose consumption on diffusion
3. The effects of cell growth within capsule
4. The ability of Comsol to solve this case by finite element method.

The overall purpose of the project is to create a tool for calculations and visualizing concentration gradient inside capsules, to be used in further research.

1.3. Limitations

The project is based on studies of literature and Farid Talebnia's PhD thesis. Such literature data will give proper mass transfer data to be able to create geometry and set boundary condition. More accurate properties calculation and assumption could improve the results.

For overcoming the computer capacity, the geometry of capsules is limited to a half of full size as axis symmetry. We look at glucose consumption as the only reaction; both growth and product formation are neglected. In reality, ethanol is produced in both exponential growth and stationary phases. The reaction in exponential growth phase is complex because of yeast growth.

1.4. Objectives

- Set up framework in Comsol Multiphysics
- Simulate sugar consumption that occurs within encapsulated yeast, which is compared to catalytic particles with three domains: membrane, liquid core and cell pellet.

2. THEORY

2.1. Encapsulated yeast

Encapsulation is designed to entrap materials such as enzyme or cells within a semi-permeable membrane which should allow the free exchange of molecules important for cell survival and function such as nutrients, oxygen, essential metabolites and toxic products of cell metabolism while retaining the larger molecular weight compounds and cells encapsulated. There are several advantages using encapsulated yeast for producing ethanol, such as higher productivity, higher ethanol yield, lower byproduct yield, high cell concentration, no lag phase, better tolerance against inhibitors, and no leakage to the media (14).

High cell concentration in the cultivation media can help decreasing the fermentation time as well as increasing the tolerance of the cells against the inhibitors [11]. Among the different methods of immobilization, cell encapsulation is promising method that probably has advantages over conventional immobilizing methods.

Microencapsulation of enzymes was pioneered [28] and later the technique was successfully applied to the animal cell culture [29]. In 1988, Nigam developed one-step microencapsulation method with calcium alginate, which was much simpler than the Lim's three-step method. Even though the conventional gel entrapment method is simple in procedure, it has a limitation in increasing biomass per unit volume of the matrix. Adding too much biomass weakens the strength of gel matrices. Also very often live cells leak out from the matrices and grow in a medium as free cells [17].

An alginate-membrane-a coating material liquid-core capsule prepared using polyethylene glycol as a thickener was produced and the intracapsular mass-transfer characteristics of glucose and proteins were investigated by Koyama and Minoru [16]. The apparent effective diffusivity of glucose into the capsule was $7.9.10^{-10}m^2/s$, which is larger than that into alginate beads ($6.5.10^{-10}m^2/s$) and in water ($6.7.10^{-10}m^2/s$) [16].

2.2. Mass transfer and reaction of encapsulated yeast

In bioprocesses, kinetics of biochemical transformation rates and mass transfer are the major regulatory phenomena. The overall rate of substrate consumption depends on the following three steps: diffusion of substrate from the bulk of the liquid to the capsule, diffusion of substrate within capsule, and biochemical reaction [20].

2.2.1. Diffusion through cell-free

For a capsule without cell inside, is only considered by diffusion phenomena. The substrate-glucose passes through the shell and fills in the whole capsule. Refer to behavior of mass transfer in spherical shell, mass balance in cell free can be formulated. It is assumed that no convection in the capsule.

Mass balance for species glucose (S) on spherical shell of thickness Δr within a single particle:

$$\begin{pmatrix} Rate\ of \\ input \end{pmatrix} - \begin{pmatrix} Rate\ of \\ output \end{pmatrix} + \begin{pmatrix} Rate\ of \\ generation \end{pmatrix} = \begin{pmatrix} Rate\ of \\ accumulation \end{pmatrix}$$

$$N_S|_r A - N_S|_{r+\Delta r} A - 0 = 0$$

$$N_S|_r 4\pi r^2 - N_S|_{r+\Delta r} 4\pi (r+\Delta r)^2 - 0 = 0$$

Division by $4\pi r^2$ and letting $\Delta r \rightarrow 0$ gives

$$\lim_{\Delta r \rightarrow 0} \frac{(r^2 N_S)|_{r+\Delta r} - (r^2 N_S)|_r}{\Delta r} = 0$$

$$\frac{d}{dr}(r^2 N_S) = 0$$

$$N_A = -\mathcal{D}\frac{dS}{dr}$$

$$-\mathcal{D}\frac{1}{r^2}\frac{d}{dr}\left[r^2\left(-\mathcal{D}\frac{dS}{dr}\right)\right] = 0$$

or

$\mathcal{D}\left(\frac{\partial^2 S}{\partial r^2} + \frac{2}{r}\frac{\partial S}{\partial r}\right) = 0$ represents for one dimensional

The governing equation above can be solved by finite element method.

2.2.1. External and internal diffusion resistance for encapsulated yeast

Substrate molecules diffuse into capsule through capsule pore. Diffusion resistance turns up from external particle diffusion and internal by 2 mechanism transfer: substrate diffuses onto membrane external surface, and then substrate diffuses through membrane to react with site active of catalyst (internal diffusion).

Substrate concentration distribution inside the capsule which containing yeast core is formulated in:

$$\begin{pmatrix} Rate\ of \\ input \end{pmatrix} - \begin{pmatrix} Rate\ of \\ output \end{pmatrix} + \begin{pmatrix} Rate\ of \\ generation \end{pmatrix} = \begin{pmatrix} Rate\ of \\ accumulation \end{pmatrix}$$

$$N_S|_r A - N_S|_{r+\Delta r} A - (-r_s')A\Delta r = V\frac{dS}{dt}$$

Division by $4\pi r^2$ and letting $\Delta r \rightarrow 0$ gives

$$\lim_{\Delta r \rightarrow 0} \frac{(r^2 N_S)|_{r+\Delta r} - (r^2 N_S)|_r}{\Delta r} - \frac{V_{max} S}{S + K_m} r^2 = r^2 \frac{dS}{dt}$$

$$r^2\frac{d^2 S}{dr^2} + 2r\frac{dS}{dr} - \frac{V_{max} S}{S + K_m} r^2 = r^2\frac{dS}{dt}$$

$$\frac{d^2 S}{dr^2} + \frac{2}{r}\frac{dS}{dr} - \frac{V_{max} S}{S + K_m} = \frac{dS}{dt}$$

By following the assumption are:

- Rate of reaction by Michaelis-Menten kinetics
- Time-dependent and distance-dependent of substrate concentration are simultaneous
- Anaerobic cultivation
- no cell growth of encapsulated cell
- Liquid core is stagnant water
- no product is produced
- moderately stirred external liquid, Sherwood number approximately 20
- cell pellet homogeneous liquid with reduced diffusivity
- no convective flux through membrane

The governing equation above can also be solved by finite element method.

3. METHOD

3.1. Finite element method

Diffusion and reaction of encapsulated yeast integrated in partial differential equation as written above. It can be solved by finite element method.

The finite element method is a numerical approach by which general differential equations can be solved in an approximate manner.

The differential equation or equations, which describe the physical problem considered, are assumed to hold over a certain region. This region may be one-, two- or three-dimensional. It is a characteristic feature of the finite element method that instead of seeking approximations that hold directly over the entire region, the region is divided into smaller parts, so-called finite elements, and approximation is then carried out each element. The collection of all elements is called a finite element mesh [19].

When the type of approximation which is to be applied over each element has been selected, the corresponding behavior of each element can then be determined. This can be performed because the approximation made over each element is fairly simple [19].

The FE method can be applied to obtain approximate solutions for arbitrary differential equations. A characteristic feature of the FE method is the region, i.e. the body, is divided into smaller parts, i.e. the elements, for which rather simple approximation is adopted. This

approximation is usually polynomial. The approximation over each element means that an approximation is adopted for how the variable changes over the element. This approximation is, in fact, some kind of interpolation over the elements, where it is assumed that the variable is known at certain points in the element. The precise manner in which the variable changes between its values at the nodal points is expressed by the specific approximation, which may be linear, quadratic, cubic, etc [19].

The starting point for the finite element method is a mesh, a partition of the geometry into small units of a simple shape, *mesh elements*.

The solution of a continuum problem by the finite element method is approximated by the following step-by-step process:

a. ***Discretize the continuum***

Divide the solution region into non-overlapping elements or sub-regions. The finite element discretization allows a variety of element shapes, for example, triangles, quadrilaterals. There is an **m** element and an **n** node. Node is a point which separates 2 elements. For 1 dimensional partial differential have 2 nodes for each element.

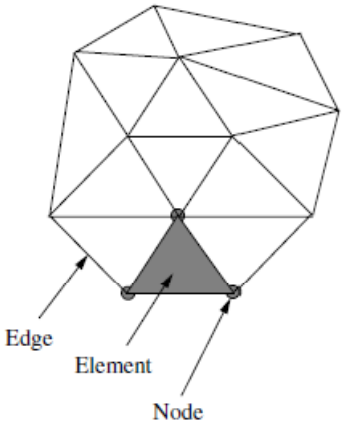

Figure 2.Typical finite element mesh. Elements, nodes and edges.

b. ***Select interpolation or shape functions***

It represents the variation of the field variable over an element.

c. ***Form element equations (Formulation)***

The term "weak form" attributes to the partial differential equations (PDE) that are to be solved. The solution of a boundary value problem described by a particular PDE can be achieved by setting the PDE to a weak form. In general the solution of a PDE can be

performed from a "strong form" or from a "weak form". The strong form description of a PDE is the one we have already known, for example the Laplace equation. Since the finite element method is based on the discretization of the domain, the solution of the strong form of the PDEs describing the problem must be descretized. For this purpose a weak form is being developed. To develop a weak form of the equations, the integration of the product of the trial functions with the equations must be performed. The trial (or test) functions are assumed to be as smooth as possible so as they vanish on the prescribed displacement boundary.

The term weak form is referred as variational form, because the solution of the PDEs is approximated with the use of trial functions. The Galerkin method is one of the methods that are based on the variational form of the equations. the variational formulation of a physical problem is often referred to as the *weak formulation*.

After briefly describing the various elements used in the context of finite element analysis, we shall now focus our attention on determining the element characteristics, that is, the relation between the nodal unknowns and the corresponding loads or forces in the form of the following matrix equation, namely,

$[\mathbf{K}]\{\mathbf{T}\}=\{\mathbf{f}\}$

where [**K**] is the thermal stiffness matrix, {**T**} is the vector of unknown temperatures and {**f**} is the thermal load, or forcing vector.

Next, we have to determine the matrix equations that express the properties of the individual elements by forming an element Left Hand Side (LHS) matrix and load vector.

For example, a typical LHS matrix and a load vector can be written as

$$[\mathbf{K}]_e=\frac{\boldsymbol{Ak}}{\boldsymbol{l}}\begin{bmatrix}1 & -1\\ -1 & 1\end{bmatrix}$$

$$\{\mathbf{f}\}_e=\begin{Bmatrix}\boldsymbol{Q_i}\\ \boldsymbol{Q_j}\end{Bmatrix}$$

where the subscript *e* represents an element; *Q* is the total heat transferred; *k* is the thermal conductivity; *l* is the length of a one-dimensional linear element and *i* and *j* represent the nodes forming an element. The unknowns are the temperature values on the nodes.

Consider the two-dimensional linear triangular elements shown in Figure 3. Let us assume the following elemental LHS matrix for the variable φ

For element 1,

$$K_1 = \begin{bmatrix} a_{11} & a_{12} & a_{13} \\ a_{21} & a_{21} & a_{21} \\ a_{31} & a_{31} & a_{31} \end{bmatrix} \quad \text{…. (3.1)}$$

And for element 2,

$$K_1 = \begin{bmatrix} b_{11} & b_{12} & b_{13} \\ b_{21} & b_{21} & b_{21} \\ b_{31} & b_{31} & b_{31} \end{bmatrix} \quad \text{…. (3.2)}$$

The elemental RHS vectors are the following:

For element 1,

$$f_1 = \begin{Bmatrix} C_1 \\ C_2 \\ C_3 \end{Bmatrix} \quad \text{...(3.3)}$$

and for element 2,

$$f_2 = \begin{Bmatrix} d_1 \\ d_2 \\ d_3 \end{Bmatrix} \quad \text{...(3.4)}$$

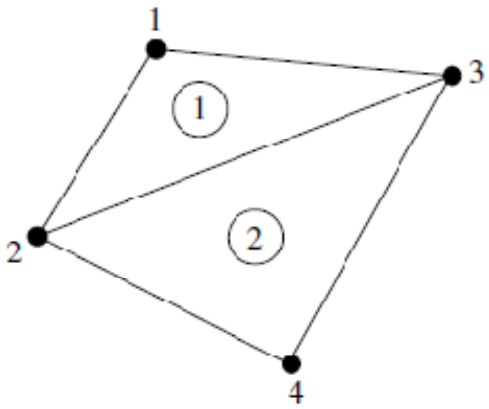

Figure 3.A domain with two linear triangular elements

d. ***Assemble the element equations to obtain a system of simultaneous equations***

To find the properties of the overall system, we must assemble all the individual element equations, that is, to combine the matrix equations of each element in an appropriate way

such that the resulting matrix represents the behavior of the entire solution region of the problem.

Assembling the above elemental contributions gives the following global equation:

$$[\mathbf{K}]\{\boldsymbol{\emptyset}\}=\{\mathbf{f}\} \quad \text{...(3.5)}$$

where [**K**] and {**f**} are the global LHS matrix and RHS vector respectively and $\{\boldsymbol{\varphi}\}$ is the unknown vector for the system shown in Figure 3 as follows:

$$\{\emptyset\} = \begin{Bmatrix} \emptyset_1 \\ \emptyset_2 \\ \emptyset_3 \\ \emptyset_4 \end{Bmatrix} \quad \text{…. (3.6)}$$

The global LHS matrix is assembled as follows. The entries with the same subscripts in Equations 3.1 and 3.2 are added together to form an assembled global LHS matrix, that is,

$$[\mathbf{K_1}] = \begin{bmatrix} a_{11} & a_{12} & a_{13} & 0 \\ a_{21} & a_{22}+b_{22} & a_{23}+b_{23} & b_{24} \\ a_{31} & a_{32}+b_{32} & a_{33}+b_{33} & b_{34} \\ 0 & b_{42} & b_{43} & b_{44} \end{bmatrix} \quad \text{... (3.7)}$$

In a similar fashion, the RHS vector is assembled as

$$\{\mathbf{f}\}=\begin{Bmatrix} c_1 \\ c_2+d_2 \\ c_3+d_3 \\ d_4 \end{Bmatrix} \quad \text{...(3.8)}$$

The global system of equations is written as follows:

$$\begin{bmatrix} \boldsymbol{a_{11}} & \boldsymbol{a_{12}} & \boldsymbol{a_{13}} & \mathbf{0} \\ \boldsymbol{a_{21}} & \boldsymbol{a_{22}+b_{22}} & \boldsymbol{a_{23}+b_{23}} & \boldsymbol{b_{24}} \\ \boldsymbol{a_{31}} & \boldsymbol{a_{32}+b_{32}} & \boldsymbol{a_{33}+b_{33}} & \boldsymbol{b_{34}} \\ \mathbf{0} & \boldsymbol{b_{42}} & \boldsymbol{b_{43}} & \boldsymbol{b_{44}} \end{bmatrix} \begin{Bmatrix} \emptyset_1 \\ \emptyset_2 \\ \emptyset_3 \\ \emptyset_4 \end{Bmatrix} = \begin{Bmatrix} c_1 \\ c_2+d_2 \\ c_3+d_3 \\ d_4 \end{Bmatrix} \quad \text{... (3.9)}$$

As seen, there are four simultaneous equations, each of them associated with a node.

The first equation, which is associated with node 1, is

$$a_{11}\emptyset_1 + a_{12}\emptyset_2 + a_{13}\emptyset_3 = c_1 \quad \text{... (3.10)}$$

In the above equation, the contributions are from node 1 and the nodes connected to node 1. As seen, node 1 receives contributions from 2 and 3. Similarly, the second nodal equation receives contributions from all other nodes, which is obvious from Equation 3.9.

e. ***Solve the system of equations***

The resulting set of algebraic equations

f. ***Calculate the secondary quantities***

From the nodal values of the field variable, for example, temperatures can be calculated the secondary quantities, for example, space heat fluxes.

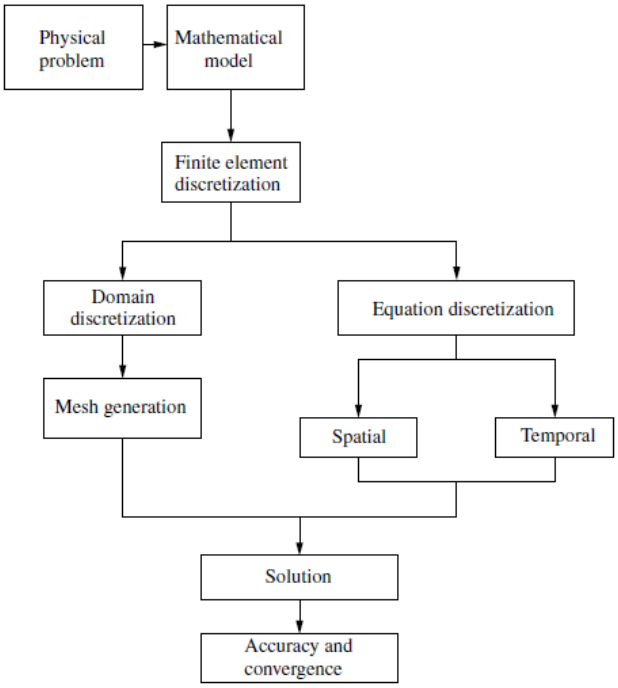

Figure 4.Numerical model for calculation in FEM

3.1.1. Two Dimensional Mass Flows

FE method is a numerical method to solve arbitrary differential equation. To achieve this objective, it is a characteristic feature of the FE approach that the differential equations are reformulated into an equivalent form, that so called weak formulation.

Weak form for is derived from strong form. The key point is the fundamental divergence theorem of Gauss.

Strong form is considered in two-dimensional body and assumed that N is the amount mass accumulated in the body per unit volume and per unit time, *C* the concentration, **D** the constitutive matrix, and *t* the thickness. The flux vector **k** is determined from Fick's law, i.e.

$Q=-\mathbf{D}\nabla C$

$$\int_A Nt\,\mathrm{d}A = \oint_L \boldsymbol{k_n} t\,\mathrm{d}L \qquad \ldots (3.11)$$

Where *t=t(x,y)* denotes the thickness in the *z*-direction of the body located in the *xy*-plane. See below

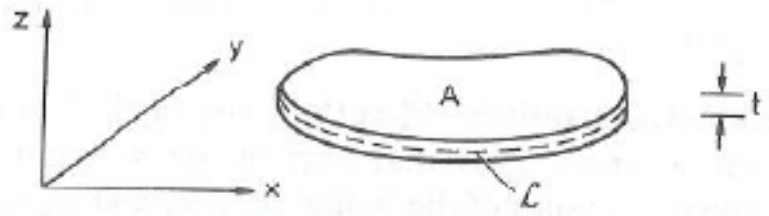

Figure 5.Two-dimensional body with thickness *t* located in the *xy*-plane

We have that $k_n = \mathbf{k}^T\mathbf{n}$. Gauss' divergence theorem yields:

$$\oint_L tk_n\mathrm{d}L = \oint_L t\mathbf{k}^T\mathbf{n}\mathrm{d}L = \oint_L (t\mathbf{k})^T\mathbf{n}\mathrm{d}L = \int_A \mathrm{div}(t\mathbf{k})\mathrm{d}A \qquad \ldots (3.12)$$

With (3.11), (3.12) takes the form

$$\oint_A [tN - \mathrm{div}(t\mathbf{k})]\mathrm{d}A = 0 \qquad \ldots (3.13)$$

$$\text{div}(t\mathbf{k}) = tN \quad \ldots (3.14)$$

which is the balance principle for the two-dimensional body. If the thickness is constant, we get

$$\text{div } \mathbf{k} = \text{N} \quad \ldots (3.15)$$

Using the constitutive equation $\boldsymbol{k} = -D\boldsymbol{\nabla}C$ in balance equation (3.14), it follows that

$$\text{div}(t\boldsymbol{D}\boldsymbol{\nabla}C) + tN = 0 \text{ in region } A \quad \ldots (3.16)$$

where region A is the entire region of the body. If the constitutive equation **D** is given by (3.17)

$$D = \begin{bmatrix} k_{xx} & 0 \\ 0 & k_{yy} \end{bmatrix}; D = \begin{bmatrix} k_{xx} & 0 & 0 \\ 0 & k_{yy} & 0 \\ 0 & 0 & k_{zz} \end{bmatrix} \quad \ldots (3.17)$$

For isotropic material, we obtain

$$\frac{\partial}{\partial x}\left(tk\frac{\partial C}{\partial x}\right) + \frac{\partial}{\partial y}\left(tk\frac{\partial C}{\partial y}\right) + tQ = 0 \quad \ldots (3.18)$$

To solve the differential equation (3.16), boundary conditions are required. These boundaries are typically of the form

$$C = g \text{ on } L_g \quad \ldots (3.19)$$

where h and g are known quantities. L_h is that part of the boundary L on which the flux q_n is known, whereas L_g is that part of the boundary L on which the concentration C is known . The sum of boundaries L_h and L_g constitutes the entire boundary L.

Show from figure below

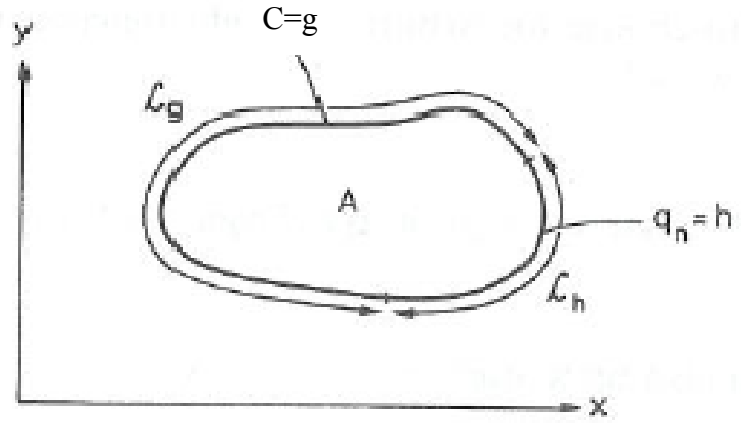

Figure 6.Two-dimensional region *A* with boundary $L=L_h+L_g$

It is possible to prediscribe the flux q_n and the concentration *C* at the same position.

With (3.16), (3.18) and (3.19) can be obtained the strong form of the mass problem:

Strong form of two-dimensional mass flow can be written by:

$\mathrm{div}(t\boldsymbol{D}\nabla C) + tQ = 0$ in region *A*

$q_n = \mathbf{q}^{\mathrm{T}}\mathbf{n} = h$ on L_h

$C=q$ on L_g

Having established the differential equation and boundary condition (strong form), will be formed the weak form.

To establish the weak form from the strong form, multiply by an arbitrary function, *v(x)* to obtain:

$$\int_A v\,\mathrm{div}(\mathbf{q}t)\mathrm{d}A - \int_A vQt\,\mathrm{d}A = 0 \qquad \text{... (3.20)}$$

Where *v=v(x,y)*. Integrating by parts the first term using the Green-Gauss theorem, we obtain:

$$\int_A v\,\mathrm{div}(\mathbf{q}t)dA = \oint_L vt\mathbf{q}^T\mathbf{n}\mathrm{d}L - \oint_A (\nabla v)^T\mathbf{q}t\mathrm{d}A \qquad \text{… (3.21)}$$

Then be rewritten in the form:

$$\int_A (\nabla v)^T \mathbf{q} t \, dA = \oint_L v \mathbf{q}^T \mathbf{n} t dL - \int_A vQt dA \quad \text{... (3.22)}$$

We may use the boundary condition to obtain

$$\int_A (\nabla v)^T \mathbf{q} t dA = \int_{L_h} vht dL - \int_{L_g} vq_n t dL - \int_A vQt dA \quad \text{… (3.23)}$$

Where h is a known quality along L_h, whereas the flux q_n is unknown along the boundary L_g.

Inserting the constitutive relation $\boldsymbol{q} = -D\boldsymbol{\nabla} C$ provides the following weak form:

$$\int_A (\nabla v)^T t D \nabla C \, dA = -\int_{L_h} vht dL - \int_{L_g} vq_n t dL + \int_A vQt \, dA \quad \text{… (3.24)}$$

$$C = g \text{ on } L_g \quad \text{… (3.25)}$$

where,

v = arbitrary weight function

D = constitutive matrix

T = temperature

t = thickness

Q = mass flow per unit time per unit volume of the body

q = flux vector (Fick's low)

From figure 6, the temperature is approximated in:

$T = \mathbf{Na}$ … (3.26)

Where **N** is global shape function matrix and **a** contains the temperature at the nodal points in the entire body. This means that

$$\mathbf{N} = [N_1 \quad N_2 \quad \dots \quad N_n]; \mathbf{a} = \begin{bmatrix} T_1 \\ T_2 \\ \vdots \\ T_n \end{bmatrix} \quad \text{… (3.27)}$$

where n is the number of nodal points for the entire body and a component N, depends on x and y, i.e. Ni = Ni (x,y). From (3.26) we obtain

$\nabla T = \mathbf{Ba}$ where $\mathbf{B} = \nabla \mathbf{N}$ … (3.28)

which implies that

$$B = \begin{bmatrix} \frac{\partial N_1}{\partial x} & \frac{\partial N_2}{\partial x} & \cdots & \frac{\partial N_n}{\partial x} \\ \frac{\partial N_1}{\partial y} & \frac{\partial N_2}{\partial y} & \cdots & \frac{\partial N_n}{\partial x} \end{bmatrix} \quad \ldots (3.29)$$

Inserting (3.28) into (3.24) gives

$$\left(\int_A (\nabla v)^T \boldsymbol{DB} t dA\right) \boldsymbol{a} = -\int_{L_h} vht\mathrm{d}L - \int_{L_g} vq_n t\mathrm{d}L + \int_A vQt\mathrm{d}A \quad \ldots (3.30)$$

The final step is to choose the arbitrary weight function v. In accordance with the Galerkin method we set

$$v = \mathbf{Nc} \quad \ldots (3.31)$$

Since v is arbitrary, the matrix c is arbitrary. From 10.11 we obtain

$$\nabla v = \mathbf{Bc} \quad \ldots. (3.32)$$

As $v = v^T$, (3.31) can also be written as

$$v = \mathbf{c}^{\mathrm{T}}\mathbf{N}^{\mathrm{T}} \quad \ldots (3.33)$$

Inserting (3.32) and (3.33) into (3.30), and nothing that c is independent of position, gives

$$c^T \left[\left(\int_A \mathbf{B}^{\mathrm{T}}\mathbf{DB} t dA\right)\mathbf{a} + \int_{L_h} \mathbf{N}^T htdL + \int_{L_g} \mathbf{N}^T q_n tdL - \int_A \mathbf{N}^T QtdA\right] = 0$$

$$\left[\left(\int_A \mathbf{B}^{\mathrm{T}}\mathbf{DB} t dA\right)\mathbf{a} + \int_{L_h} \mathbf{N}^T htdL + \int_{L_g} \mathbf{N}^T q_n tdL - \int_A \mathbf{N}^T QtdA\right] = 0 \quad \ldots (3.34)$$

which is the FE formulation sought.

To write (3.34) in a more compact fashion, we define the following matrices:

$$\mathbf{K} = \int_A \mathbf{B}^{\mathrm{T}}\mathbf{D}\mathbf{B}t\mathrm{d}A$$

$$\mathrm{f_b} = -\int_{L_h} \mathbf{N}^T \mathrm{h}t\mathrm{d}L - \int_{L_g} \mathbf{N}^T q_n t\mathrm{d}L \qquad \ldots (3.35)$$

$$\mathrm{f_1} = \int_A \mathbf{N}^{\mathrm{T}} Q t\mathrm{d}A$$

As **D** has the dimension 2 x 2 and **B** the dimension 2 x *n*, it follows that **K** is a square matrix with dimension *n* x *n* and it is the *stiffness matrix*. Likewise, both $\mathbf{f}_b$ and $\mathbf{f}_l$ have the dimension *n* x 1 and they are termed the *boundary vector* and *load vector*, respectively.

$\mathbf{K}a = \mathbf{f}_b + \mathbf{f}_l$ … (3.36)

We define the force vector **f** by

$\mathbf{f} = \mathbf{f}_b + \mathbf{f}_l$ … (3.37)

(3.36) becomes

$\mathbf{K}\mathbf{a} = \mathbf{f}$ … (3.38)

Region A with thickness t, the balance principle states that

$$\int_A Q t dA = \oint_L q_n t dL \ldots (3.39)$$

$f = f_b + f_l$, $i = 1,\ldots,n$ …(3.40)

$$\sum_{L=1}^{n} f_L = \sum_{L=1}^{n} f_{bi} + \sum_{l=1}^{n} f_{li} \qquad \ldots (3.41)$$

According to (3.35) we have that

$$f_b = -\int_{L_l} N_i h t\mathrm{d}L - \int_{L_g} N_i q_n t\mathrm{d}L \qquad \ldots (3.42)$$

We recall that the boundary condition specify the flux q_n=h along L_h whereas the flux q_n along L_g is unspecified beforehand. Therefore, (3.42) may be written as

$$f_{bi} = -\oint_L N_i q_n t dL \qquad \ldots (3.43)$$

From (3.35) a component of the load vector is given by

$$f_{li} = -\int_L N_i Q t dA \qquad \ldots (3.44)$$

Using (3.42) and (3.43) leads to

$$\sum_{i=1}^{n} f_i = \oint_L \left(\sum_{i=1}^{n} N_i\right) q_n t \mathrm{d}L + \int_A \left(\sum_{i=1}^{n} N_i\right) Q t \mathrm{d}A$$

$$\sum_{i=1}^{n} f_i = \oint_L q_n t \mathrm{d}L + \int_A Q t \mathrm{d}A \qquad \ldots (3.45)$$

A comparison with (3.39) shows that

$$\sum_{i=1}^{n} f_i = 0$$

This means that the balance principle for the body is expressed by the fact that the sum of the components of the force vector f is equal to zero. We emphasize that (3.45) holds exactly even though the finite element method is an approximate approach.

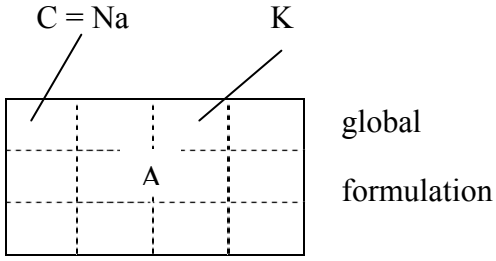

3.2.1. Convergence and Order Mesh Quality

The FE method provides an approximate solution to the problem at hand and it is obvious that the more elements we use the more accurate the approximate solution. In the limit, when the elements are infinitely small, we require that our approximate solution is infinitely close to the exact solution. This is the convergence requirement [19].

The first step in an FE analysis is to select the type of elements and corresponding FE mesh. There are no fixed rules on how to make these decisions. Clearly, for a given type of element the accuracy increases with decreasing element size and, in general, one will use small elements in regions where the unknown function- the concentration-varies rapidly[19].

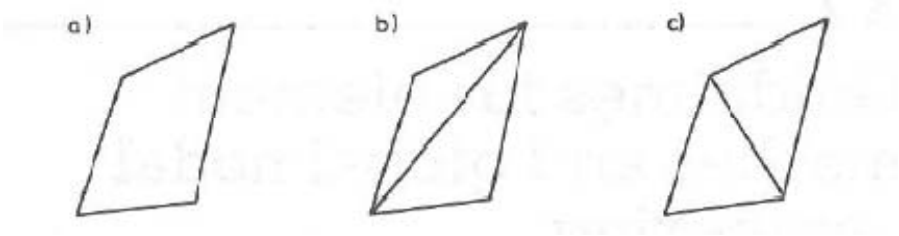

Figure 7. a) Quadrilateral; b) Interior division; c) Desirable division

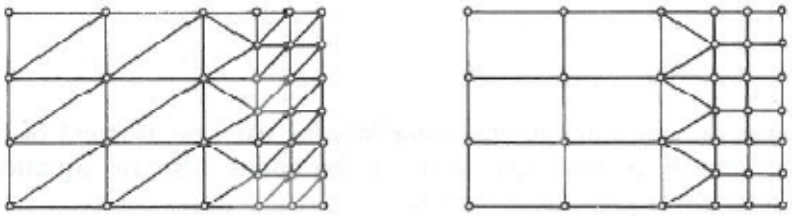

Figure 8.Mesh refinement

In order obtain an efficient solution scheme, we want to use few elements in regions where the unknown function varies slowly, but many elements in regions where it varies rapidly. Two possibilities, which allow for such a mesh refinement and which fulfill the continuity requirement, are illustrated in fig. 8 for the three-node triangular element and four-node rectangle.

It is obvious that the division in fig. 7(c) is better than that of 7(b), since the largest dimension of the elements in 7(c) is smaller than that given by 7(b). The ratio between the largest and the smallest dimension of an element is called the aspect ratio and in a good FE mesh, the aspect ratio is as close as possible to unity.

The convergence order is a measure for the improvement of the solution as a consequence of mesh refinement. In order to determine the convergence order from numerical runs, the errors of runs with different refinement level have to be related.
The convergence of a numerical solution of one or several partial differential equations generally depends on various characteristics of the problem, on the numerical algorithm, on the mesh refinement and on the mesh quality. Solving the same problem with finer grid and seeing the variation in result is a good way to analyze grid independence.

3.2. Simulation in Comsol Multiphysics

The diffusion module of Comsol Multiphysics was used to solve the encapsulated cell problem. There are some step for modeling and simulating in Comsol.

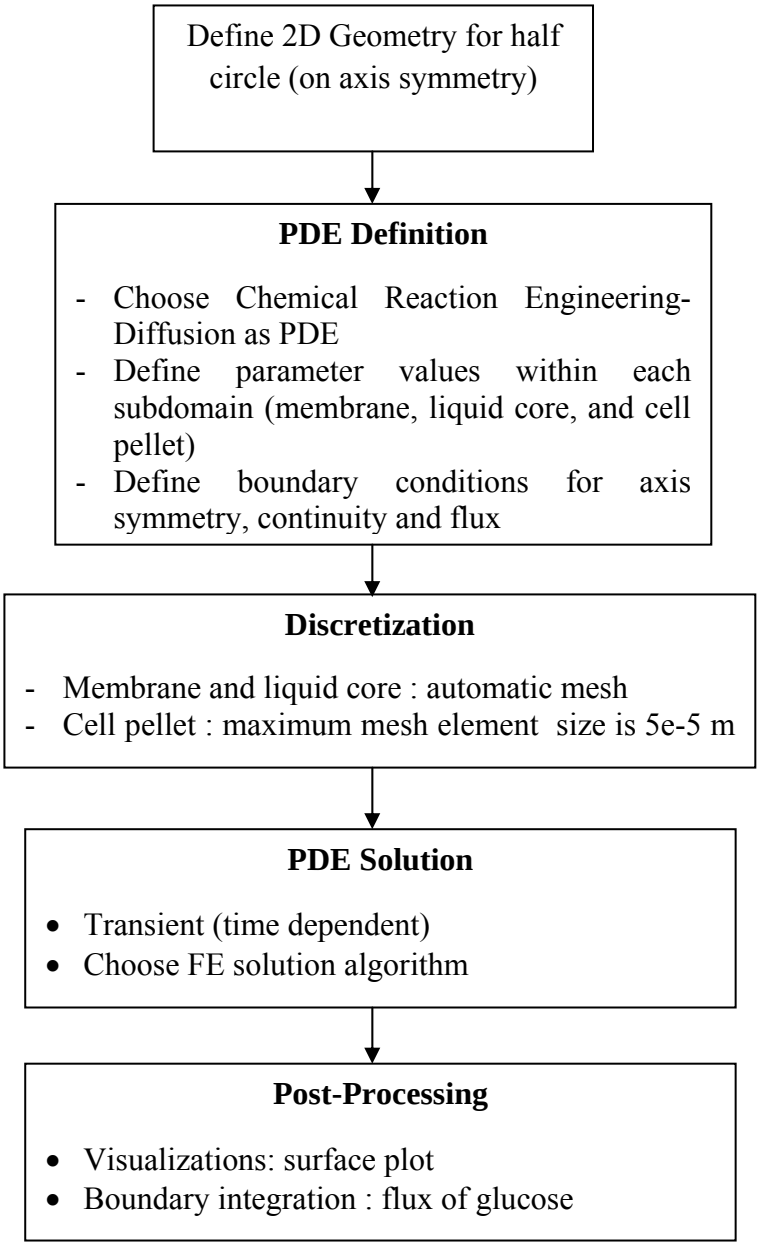

Figure 9.Steps in Comsol simulation

3.2.1. Geometry and Mesh

This model introduces the concept of effective diffusivity in yeast encapsulated in spherical porous membrane. Glucose passed through the membrane into capsule by diffusion. Capsule was divided into three sections, which were membrane, liquid core and cell pellet. Capsule had ca. 3.5 mm of diameter and 0.17 mm of thickness.

A simple geometry with a sphere was modeled to develop a model with acceptable results. The aim was to decide which solver parameters and boundary conditions to use. The model may not be exact like reality due to those assumptions. Inhibitor effects were not taken into consideration.

Meshing was in free mesh parameters by including maximum element size. Free mesh parameters can specify local mesh-element sizes and control the element distribution. Mesh must be prescribed until we have grid independence and reach convergence. The case was set up in 2D only. A symmetry axis was used to make the simulation run faster.

Comsol was used as software to create geometry and mesh, see figure 8The mesh in regions of specific interest was adjusted. The interesting region was the pellet region in which the mesh looked finer than in the others 2 subdomains. Maximum element size in membrane and liquid core was set equal to the initial, and maximum size in cell pellet was 5e-5 m. The mesh had to be irregular for it to be possible to generate a mesh. It was examined in Comsol if there were any cells with high level of skewness. The number of cell in the mesh with no cell was 281 elements, with 25%-cell pellet was 1720 elements, with 50%-cell pellet was 3337 elements, with 75%-cell pellet was 5010 elements and in the mesh without liquid core was 6155 elements.

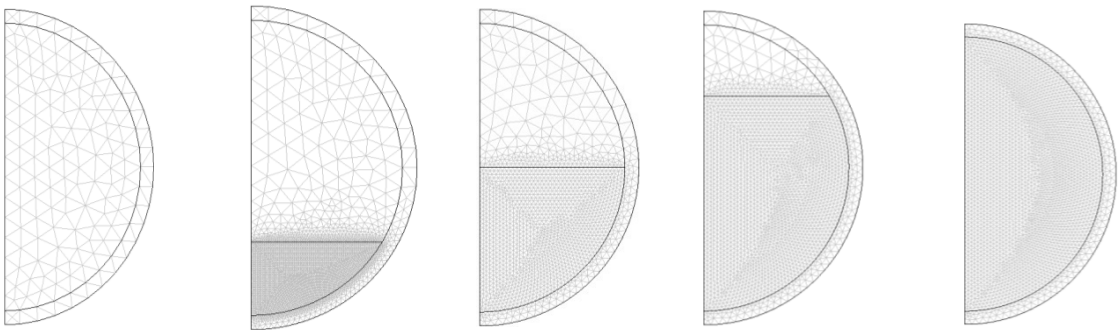

(a) (b) (c) (d) (e)

Figure 10.Mesh with no cell, 25%, 50%, 75%, and 100% of cell-filling

The artificial porous structure used in this model is depicted in Figure 11 below.

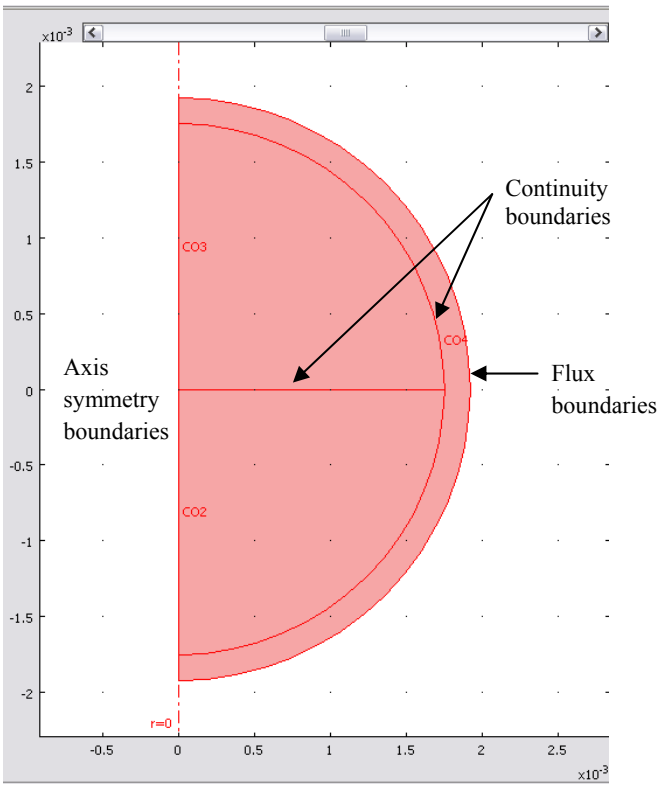

Figure 11.Artificial porous structure

Figure 11 shows the three subdomains. Membrane subdomain is CO4, liquid core is CO3, and cell pellet is CO2.

3.2.2. Model Definition and settings

The process that was simulated was the change in the concentration profiles in a capsule which occurs when encapsulated cells react with glucose when the capsule is dipped into a well-stirred glucose solution. Glucose passes through membrane and reacts in cell section.

The model equation in the modeled domains shown in Figure 11 is the time-dependent equation

$$\frac{dc_s}{dt} + \nabla.(-D\nabla c_s) = R \qquad (3.2.2.a)$$

where C_s denotes concentration (mol/m^3 using SI units), D the diffusion coefficient (m^2/s) of the solute and R the reaction rate (mol/m^3.s).

Reaction rate is Monod equation,

$$R(c) = \frac{V_{max}.c_s.c_c}{K_s + c_s} \qquad (3.2.2.b)$$

The boundary conditions are of 3 different types. A flux boundary condition applies at capsule surface boundary in Figure 11. It is expressed as

$$-n.N = N_0 + k_c(c_b - c)\ ; N = -D\nabla c \qquad (3.2.2.c)$$

where n is the normal vector to the boundary, C is a concentration in every step. In the equation for the flux condition, N_0 is an arbitrary user-specified flux expression. In this case, N_0 was set to 0. Furthermore, k_c represents the mass transfer coefficient and c_b is the bulk concentration in the fictitious diffusion layer at the boundary.

The conditions at the inner boundaries in Figure 11 were set as continuity, according to

$$n.(N_1 - N_2) = 0;\ N_i = -D_i\nabla c_i \qquad (3.2.2.d)$$

This is the default boundary condition on interior boundaries and pair boundaries; it is not applicable to exterior boundaries. The vertical boundary was considered to have axial symmetry, according to

$$n.(-D\nabla c) = 0 \qquad (3.2.2.e)$$

The axial symmetry condition is identical to the insulation/ symmetry condition. However, the axial symmetry allows generation of 3D simulation by rotation.

As described above about model equation, diffusion and reaction model is straightforward to solve this problem. Diffusion was approximated by constant diffusion coefficients of substrate in the surface membrane, liquid core and cell pellet, respectively. Reaction was approximated by Monod equation.

Diffusion and reaction equation was calculated from properties in Table 1.

Table 1.Diffusion and reaction properties

Properties	Symbol	Value	Unit
d_{inside}-capsule	d_c	3.5	[mm]
Capsule thickness	t_c	0.17	[mm]
Michaelis-Menten constant	Vmax	$1.80556.10^{-6}$	[mol/m^3.s]
Monod constant	Ks	1	[mol/m^3]
Glucose concentration	c_S	1000	[mol/m^3]
Cell concentration 325 g DW/L Molecule weight = 25.6 g/C-mol	c_X	12965.3	[C-mol/m^3]
Substrate diffusivity in water	Dw	$6.9.10^{-10}$	[m^2/s]
Sherwood number	Sh	20	dimensionless

3.2.3. Solver

Seeing the rather simple geometry and low number of mesh cells, a direct solver could be used. In Comsol this is typically UMFPACK. Alternatively PARDISO may be used, but is generally used on larger systems. UMFPACK requires more memory during computations, while PARDISO does not, but instead requires longer computational time.

It solves general systems of the form $Ax = b$ using the nonsymmetric-pattern multifrontal method and direct LU factorization of the sparse matrix A. It employs the COLAMD and AMD approximate minimum degree preordering algorithms to permute the columns so that the fill-in is minimized. The code, written in C, uses level-3 BLAS (Basic Linear Algebra Subprograms) for optimal performance [15].

4. RESULT AND DISCUSSION

4.1. Variation of diffusivities

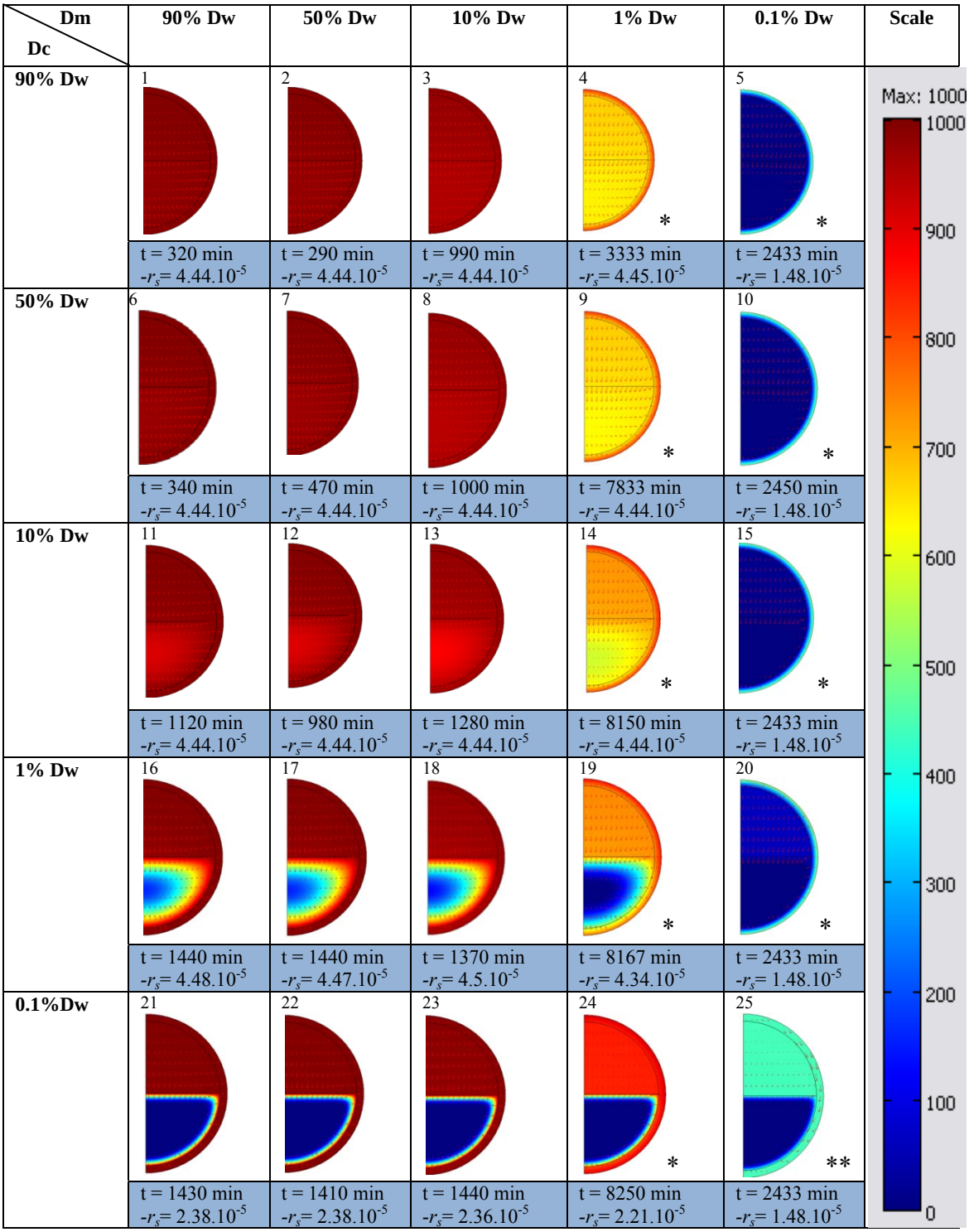

Figure 11.Simulated concentration profiles of glucose for variation of Dm and Dc glucose addition to the surrounding medium.

Design 14 and 18 in Figure 11 had close to maximum overall reaction rate, but the concentration profiles looked quite different, and it took longer time for design 14 to reach steady state. Since it takes some time before glucose can diffuse into the center of the core, it is likely that there are zones of low glucose concentration when the glucose is first added. To investigate this, the concentration profiles at 1, 2 and 6 h were calculated (Figure 13).

Dw, Dm and Dc are the diffusivities in water, membrane and cell pellet, respectively; t: time to reach steady state concentration profile; r_s: integrated glucose flux across the membrane at steady state. As an exception, the capsule which has one star icon means that the capsule needs the long time to reach steady-state and two stars icon means that steady-state could not be reached within 24 h.

In Figure 12, the glucose concentration profiles after 24 h at 50% cell pellet filling are shown depending on various combinations of diffusivities in the capsule membrane and in the cell pellet.

At high Dc (90% of Dw, 50%-Dw, 10%-Dw), the inside of the capsule still had a high concentration of glucose, shown in red in the surface plot. This means that diffusion was rapid enough to compensate for all glucose consumption, and the glucose consumption rate was at its maximum in the whole cell pellet.

At small Dc (1% and 0.1%-Dw), there was a concentration gradient of glucose, as indicated by changing in the color plot. The small Dc caused more visible changes in the concentration within the capsule.

On the other hand, small value of Dc means that it took a long time for the glucose to reach the cell pellet, to react. The time, needed to reach a steady-state concentration profile was over 24 hours.

Change of Dm did not cause any significant change to the concentration gradient, only to the overall concentration level. This indicates that diffusivities in the cell pellet-Dc were rather more important than the diffusivity of the membrane capsule.

The relationship between rate ($-r_s$) and glucose concentration is that the glucose concentration must be very low before the rate actually decreases. If S=20*Ks then r=20/21*Vmax and if S=5*Ks then r=5/6*Vmax. The scale for 0-5 mmol/L and 0-20 mmol/L can be shown below.

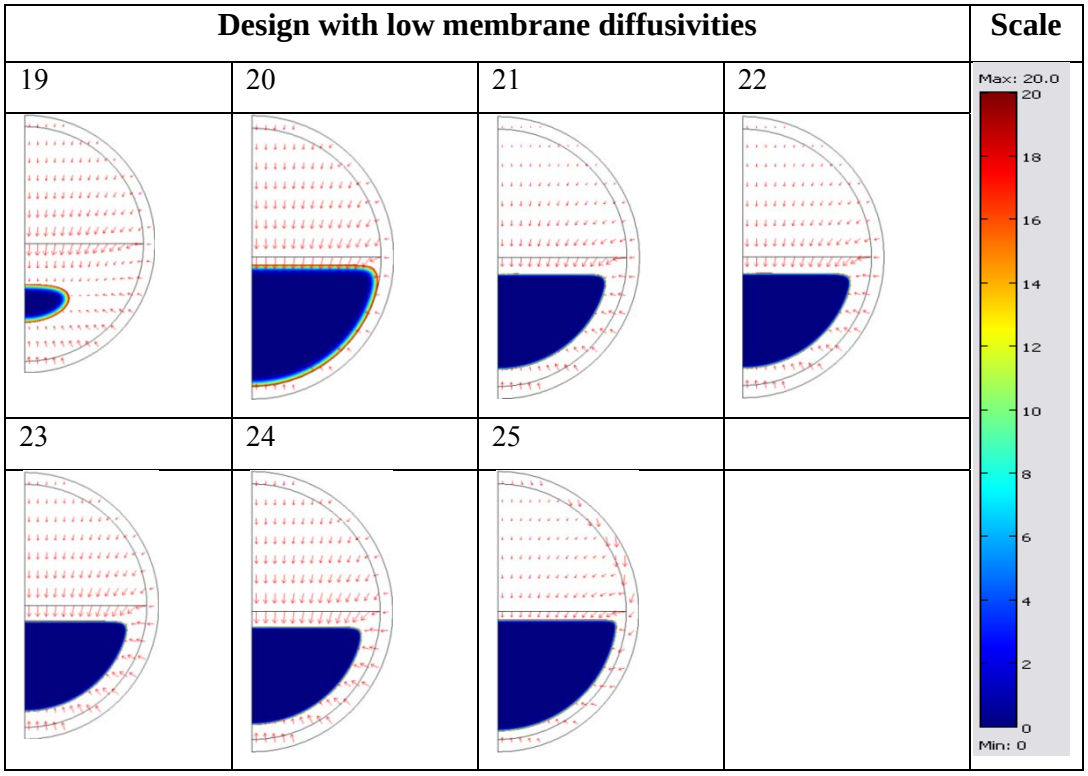

Figure 12.Diffusion limitation of Design 19-25 at concentration of glucose < 20 mol/m^3. Glucose limitation was defined as $S<5*K_S$, corresponding to $V<83\%$ of V_{max}.

At figure 11, the maximum overall reaction rate on design 14 and 18 is almost similar. Both glucose concentration profiles and the time to reach steady-state are quite different. It can be assumed that there are zones where the glucose diffuses into the center of core very slowly at the first added. This case can be investigated by looking at concentration profiles during 1, 2 and 6 first hour.

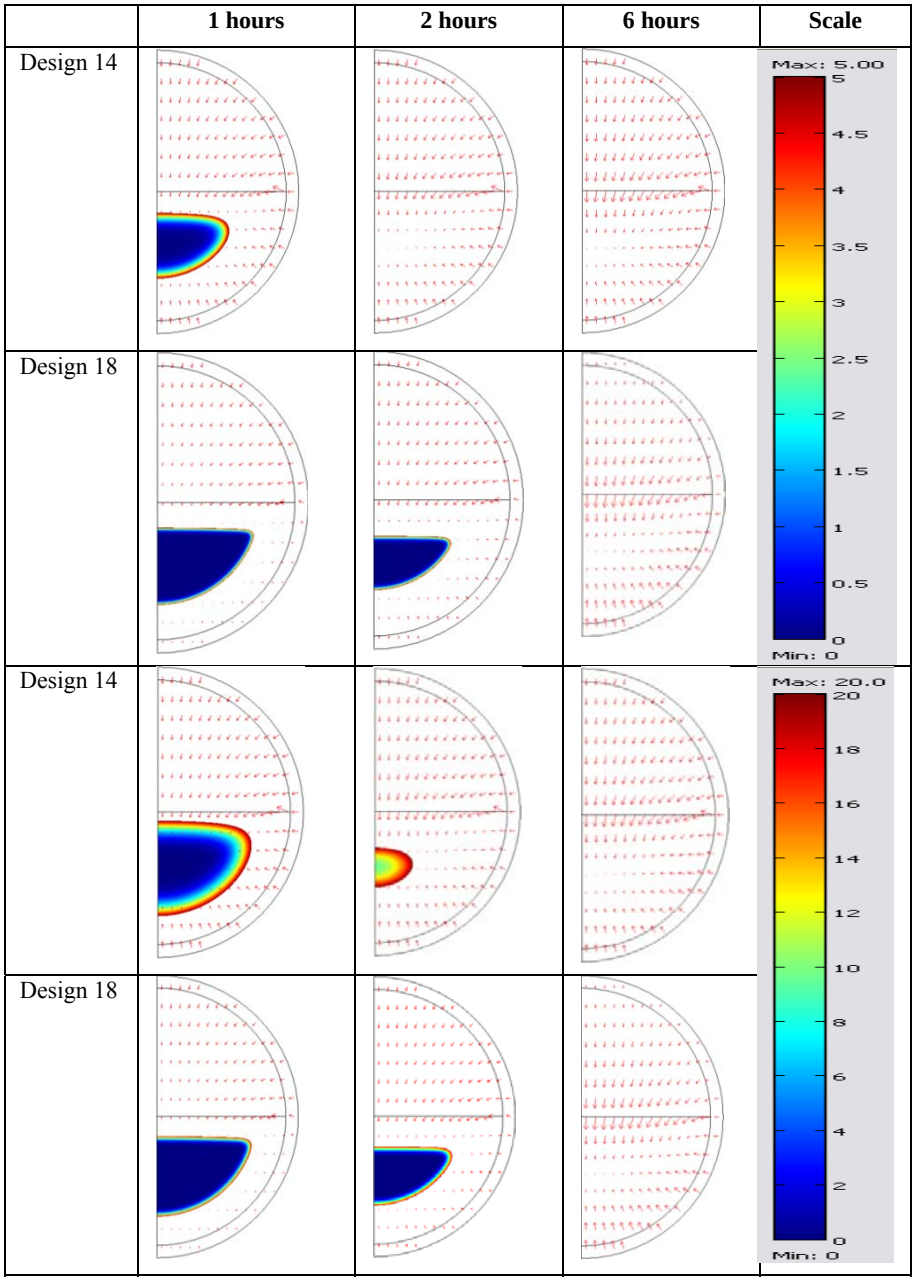

Figure 13.Concentration profile of glucose at different time of cultivation.

Design 14 with Dm = 6.9e-12 and Dc = 6.9e-11 had a zone with lower than 5 mol/m^3 of glucose concentration at 1 hours cultivation. There was still a zone below 20 mol/m^3 of glucose at 2 hours cultivation.

Design 18 with Dm = 6.9e-11 and Dc = 6.9e-12 had larger zones below 5 mol/m^3 of glucose at 1 hours cultivation and below 20 mol/m^3 of glucose at 2 hours cultivation.

Despite the lower Dm, concentration of glucose at Dc= 6.9e-11 (design 14) is higher than concentration at Dc= 6.9e-12 (design 18). At Dc= 6.9e-12 only little glucose was available within the cell pellet during the first hours.

Diffusion limitation can be analyzed from this part. Thus, at Dc= 6.9e-11 or lower, diffusion limitation leads to glucose limitation during the first few hours of cultivation.

4.2. Variation of Cell-filling

The glucose concentration profile not only depend on the diffusion of the glucose but also on the size of the cell pellet, since this will both affect the rate of reaction and the diffusion distances. Therefore, the concentration profiles at different degrees of cell filling were calculated at two combinations of membrane and cell pellet diffusivities.

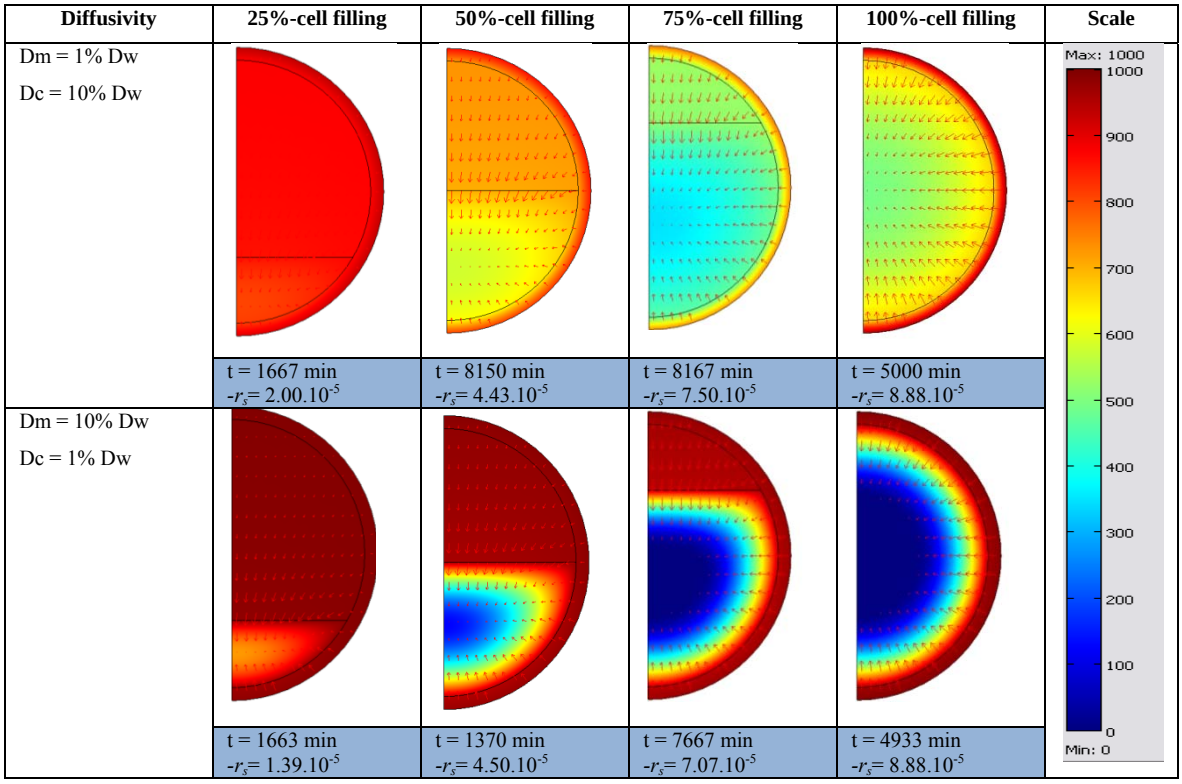

Figure 14.Concentration profile of different cell-filling at 24 hours cultivation

In these two combinations, the overall reaction rate is higher the more cells are in the capsule. Nevertheless, there were low levels in the center of the larger cell pellets. Reaction rate is higher with increasing cell filling. At 50%-cell filling concentration profile, gradient concentration seems to be more stable than others. The smallest cell filling has higher glucose concentration in cell pellet whereas the biggest cell filling has lower glucose concentration in cell pellet.

At 50% cell-filling shows more stable concentration profile. I can be assumed that cell and the glucose has a more convenience space to react each other.

It is interesting to look at the concentration profile for several cell-filling at 1, 2 and 6 h to investigate how glucose concentration depends on its diffusion into center core.

The glucose concentration can be investigated by looking at 1, 2 and 6 h after glucoses added.

Glucose Limitation	Filling	1 hours	2 hours	6 hours	Scale
5 mmol/L	50%	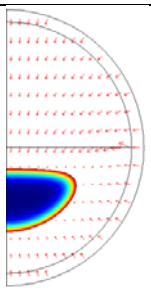	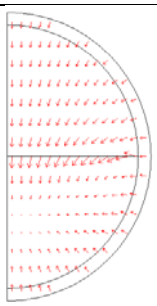	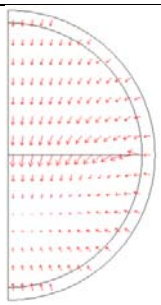	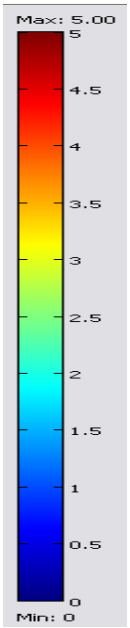
	75%	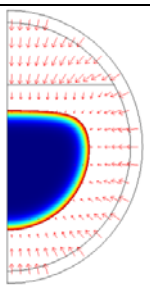	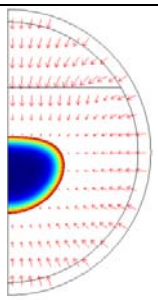	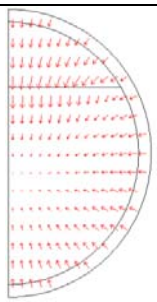	
	100%	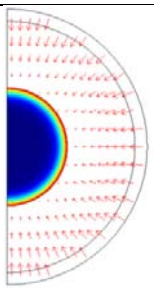	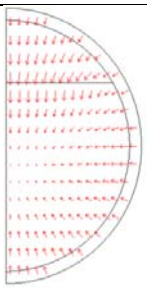	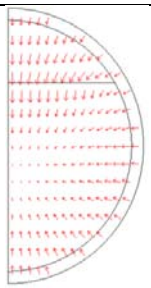	

Figure 15a.Concentration profile of glucose for different cell-filling at different time of cultivation for Dm = 1% Dw; Dc = 10% Dw and scaling for 0-5 mmol/L

Glucose Limitation	Filling	1 hours	2 hours	6 hours	Scale
20 mmol/L	50%	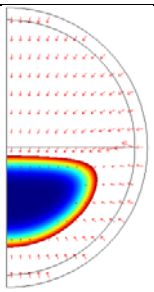	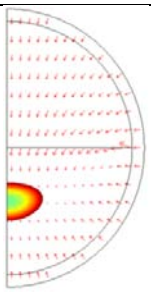	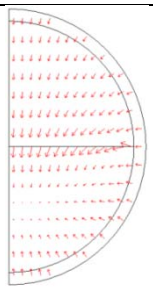	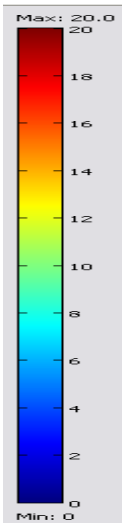
	75%	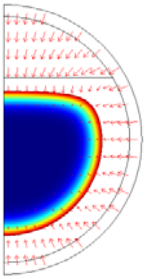	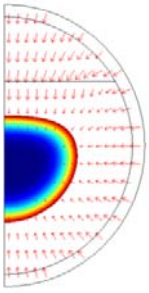	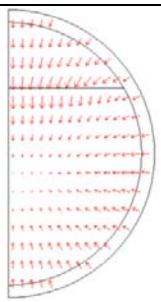	
	100%	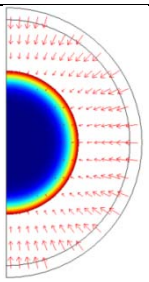	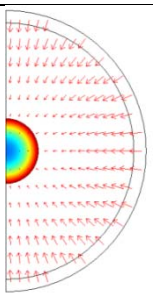	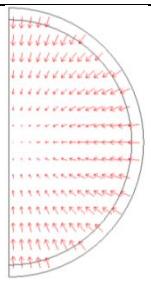	

Figure 15b.Concentration profile of glucose for different cell-filling at different time of cultivation for Dm = 1% Dw; Dc = 10% Dw and scaling for 0-20 mmol/L

Diffusion limitation for scale 0-5 mmol/L and 0-20 mmol/L are showed in 50-100% cell-filling during 1 and 2 hour at the first glucose added.

It means that at this time, the rate decreases after the glucose concentration in the 5 and 20 mmol/L.

In cultivations performed by Talebnia, glucose was converted within 10 h without significant lag phase [7]. Due to the diffusivity in cell pellet gives the diffusion limitation during the cultivation.

Glucose Limitation	Filling	1 hours	2 hours	6 hours	Scale
5	25%	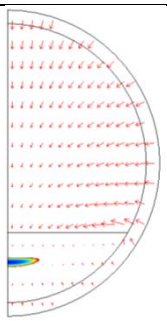	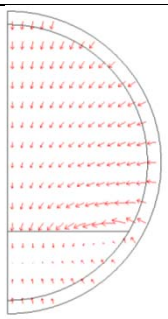	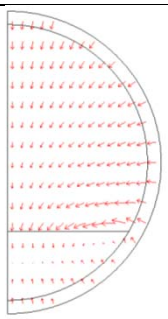	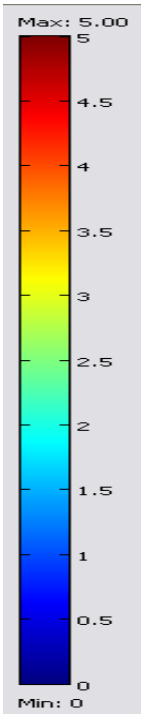
	50%	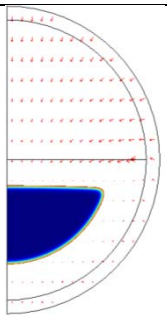	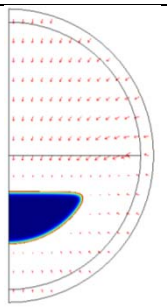	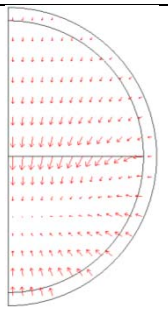	
	75%	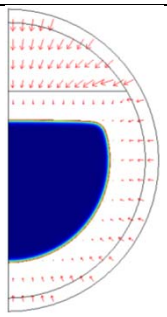	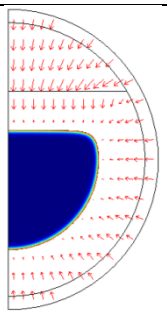	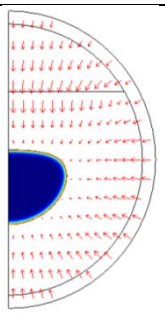	
	100%	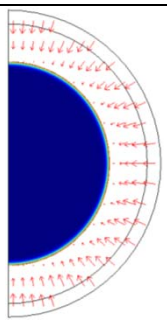	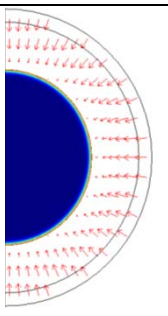	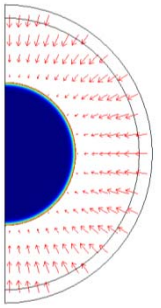	

Figure 15c.Concentration profile of glucose for different cell-filling at different time of cultivation (Dm = 10% Dw; Dc = 1% Dw), scaling for 0-5 mmol/L

Glucose Limitation	Filling	1 hours	2 hours	6 hours	Scale
20	25%	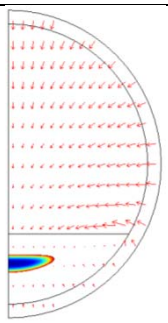	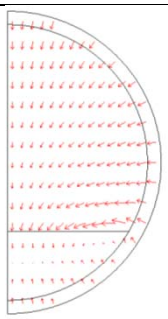	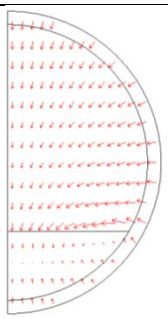	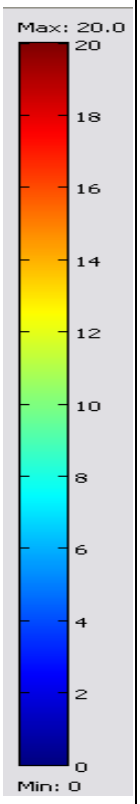
	50%	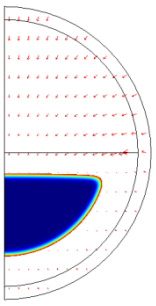	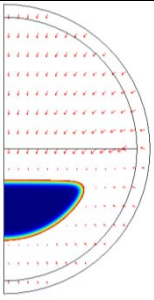	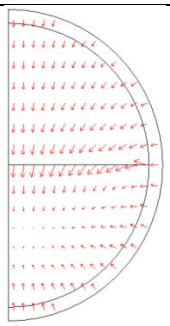	
	75%	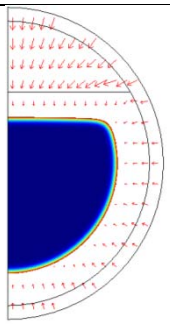	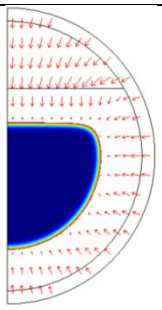	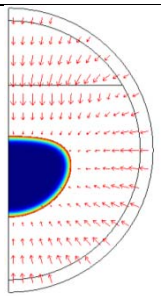	
	100%	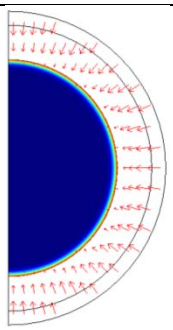	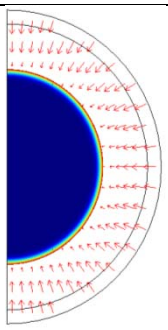	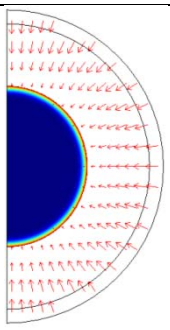	

Figure 15d.Concentration profile of glucose for different cell-filling at different time of cultivation (Dm = 10% Dw; Dc = 1% Dw), scaling for 0-20 mmol/L

For 25%-cell filling, Figure 15 shows low rate of glucose consumption, but it took short time to reach steady-state condition. At higher cell-filling, longer time was needed to reach steady-state condition but the final rate of glucose consumption was higher, despite the large diffusion limited zones.

5. Conclusions

There are several things to conclude for this case, that is:

a. A framework for simulating concentration profiles in yeast capsules has been created. Comsol can solve this case by chemical reaction engineering multiphysics. It is difficult to validate exact value within the capsule. The solver is in qualitative result properly, which shows from surface plot (concentration profile).
b. By making combination of Dm and Dc value gives the effect for rate limiting concentration during a few hours after glucose addition. The longer time to rech steady state is needed when the cell pellet was <1%.
c. The diffusion phenomena of glucose through the capsule are influenced by external and internal diffusion. The external diffusion which represent from membrane of capsule doesn't affect the rates very much. In the other hand, the internal diffusion, specifically for cell diffusivity affects the rate very much. A 50% of cell-filling is more stable of concentration profile than other, it can also be caused by electrostatic, hydrophobic or hydrophilic from substrate and capsule.

6. Future Outlook

This work is still very simple, for modeling and simulation. For future work I suggest:

a. Include inhibitor effects in the reaction kinetics.
b. Keep working in Comsol for simulation by including cell growth
c. Look for ways of validating concentration profiles with experimental studies
d. Make a complete simulation to CFD for greater system. Look at CFD effect of glucose transportation pass through into encapsulated yeast during the cultivation in continuous stirrer tank reactor by turbulence assumption

REFERENCES

1. **Bai, F. W**., et al.,. *Ethanol Fermentation technologies from sugar and starch feedstock*. Biotechnology Advanced **26**: 89-105, 2008

2. **Azhar, A.F., Bery, M. K., Colcord, A. R., Roberts, R. S., and Corbitt, G. V**.: *Factors affecting alcohol fermentation of wood acid hydrolyzate*. Biotechnol. Bioeng. Symp., 11: 293-300 , 1981.

3. **Cbung, I. S. and Lee, Y. Y**.: *Ethanol Fermentation of Crude Acid Hyrolyzate of Cellulose Using High-Level Yeast Inocula*. 2nd edition. Academic Press, San Diego,1993.

4. **A. Martinez, M.E. Rodriguez, M.L. Wells, S.W. York, J.F. Preston and L.O.Ingram**, *Detoxification of dilute acid hydrolysates of lignocellulose with lime, Biotechnol Progr 17*, p. 287–293,2001

5. **Talebnia, F and M.J. Taherzadeh**. *In situ detoxification and continuous cultivation of dilute-acid hydrolyzate to ethanol by encapsulated S. cerevisiae*, J Biotechnol 125, p. 377–384, 2006.

6. **Licht, F.O. 2006**. World Ethanol Market: The Outlook to 2015, Tunbridge Wells, Agra Europe Special Report, UK.

7. **Talebnia, F.** *Ethanol Production from Cellulosic Biomass by Encapsulated Saccharomyces cereviseae*.Chalmers University of Technology, Dep. of Chemical and Biological Engineering,2008..

8. Palmqvist, E., Hahn-Hagerdal, B., 2000b. Fermentation of lignocellulosic hydrolysates. II: inhibitors and mechanisms of inhibition. *Bioresource Technology* **74**: 25–33..

9. Talebnia, F., Niklasson, C., and Taherzadeh, M.J., 2005. Ethanol Production From Glucose and Dilute-Acid Hydrolyzates by Encapsulated *S. cereviseae*. Biotechnol Bioeng **90(3)**:345-53.

10. **Nielsen, J,**Bioreaction engineering principles.—2nd ed/ Jens Nielsen, John Villadsen and Gunnar Liden. ISBN 0-306-47349-6, 2002.

11. **Chung and Lee, 1985.** I.S. Chung and Y.Y. Lee , Ethanol production of crude acid hydrolysate of cellulose using high level yeast inocula. *Biotechnol. Bioengng.* **27** (1985), pp. 308–315

11. **Fogler, H. Scott**. Elements of Chemical Reaction Engineering. u.o : Pearson Education, 2006, 4th edition.

12. **Matthias K. Gobbert** . Alginate as immobilization matrix for cells. TIBTECH-MARCH 1990. Vol. 8, p.75-76. 2001-2008.

13. **Anderson, Bengt**, **Ronnie Andresson, Love Håkansson, Mikael Mortensen, Rahman Sudiyo, Berend van Wachem**. Computational Fluid Dynamics for Chemical Engineers. Gotheburg: u. n., 2008.

14. Talebnia, F., C., Taherzadeh, M.J. (2007): *Physiological and Morphological Study of Encapsulated Saccharomyces cerevisiae*, **Enzyme Microb. Technol.,** 41(6-7): 683-688

15. **Comsol AB**. Comsol Multiphysics 3.5a Documentation. 2008

16. **Koyama, K and Minoru, S**. *Keitaoroevaluation of mass-transfer characteristics in alginate-membrane liquid-core capsules prepared using Polyethylene Glycol*, 98(2):p.114, 2004.

17. Cheong SH, Park JK, Kim BS, Chang HN. 1993. Microencapsulation of yeast cells in calcium alginate membrane. *Biotechnol Tech* **7**: 879-884.

18. **Tanaka, H., Matsumura, M., and Veliky, I. A.**, *Diffusion characteristic of substrate in Ca-alginate gel beads*. Biotechnology and Bioengineering, 26(1): p 53-58, 2004.

19. **Ottosen, N and Peters on, H**., *Introduction to finite element methods*. Pearson Prentice Hall. 1992;p.81-85,91223

20. **Hamdi, M.** *Biofilm thickness effect on the iffusion limitation in the bioprocess reaction: Biofloc critical diameter significance.* Bioprocess engineering,p. 193, 1995.

21. Wijayanti, Sri, *Evaluation of an Alginate-Chitosan-Microcrystalline Cellulose Sulfate Macroencapsulation System for Efficient Fermentation of Lignocellulosic Hydrolyzate ,* Master of Science Thesis in Industrial Biotechnology, Chalmers, 2009.

22. Chang, H. N., et al., 1996. Microencapsulation of recombinant *Saccharomyces cerevisiae* cells with invertase activity in liquid-corenalginate capsules. *Biotechnology and Bioengineering* **51**: 157-162.

23. Park, J. K., and Chang, H. N., 2000. Fermentation of lignocellulosic hydrolysates for ethanol production. *Enzyme and Microbial Technology* **18**: 312-331.

24. Delgenes J.P. Moletta R.; Navarro J.M., 1996. Effects of lignocellulose degradation products on ethanol fermentations of glucose and xylose by *Saccharomyces cerevisiae, Zymomonas mobilis, Pichia stipitis*, and *Candida shehatae*. *Enzyme and Microbial Technology* 19 : 220-225

25. Lynd, L.R., 1996. Overview and evaluation of fuel ethanol from cellulosic biomass: technology, Economics, the Environment, and Policy. *Annual Review of Energy and the Environment* **21**: 403–465.

26. Orive, G., et al., 2004. Histrory, challenges and perpectives of cell microencapsulation. *Trends in Biotechnology* **22**: 87-92.

27. Bhatia, S. R., et al., 2005. Polyelectrolytes for cell encapsulation. *Current Opinion in Colloid & Interface Science* **10**: 45-51.

28. Chung. 1972. Effects of Local Applications of Microencapsulated Catalase on the Response of Oral Lesions to Hydrogen Peroxide in Acatalasemia. Journal of Dental Reserch: 319-321

29. Lim, F. and Sun, A.M., Microencapsulated islets as bioartificial endocrine pancreas. ***Science,*** 210 (1980) 908-910.

30. Lewis, R. W. and Perumal, N. Fundamentals of the Finite Element Method for Heat and Fluid Flow. Wiley.